

A Viscoelastic Model for Droplet Breakup in Dense Emulsions

Joseph D. Peterson¹, Ioannis Bagkeris², Vipin Michael³

¹Henry Samueli School of Engineering, UCLA, Boelter Hall, 4531J

²Unilever R&D, Port Sunlight Laboratory, Quarry Road East, Bebington, Wirral
CH63 3JW, UK

³School of Engineering, University of Manchester, Manchester, M13 9PL, UK
May 29, 2023

Abstract

When processing dense emulsions, complex flows stretch and deform droplets to the point of breakup, changing the droplet size distribution and the mechanical properties of the final product. For steady homogeneous flows, a droplet’s shape and proclivity to breakup can be inferred from a Capillary number, comparing the strain rate with the typical shape relaxation time. More generally, a droplet’s shape depends on its whole history of deformation, and this distinction can be salient under conditions relevant to industrial processing. Here, we develop a coupled population balance and droplet shape evolution model “STEPB” with a breaking rate determined by the droplet’s shape. In a first application of the STEPB model, we consider droplet breakup during relaxation of step shear, where we predict non-trivial strain-dependent final daughter droplet distributions. We also compare predictions from STEPB against experimental observations in steady flow conditions, illuminating key weaknesses in the model due to neglected terms.

1 Introduction

Dense emulsions are stabilized mixtures of immiscible or partially miscible fluids, comprising a dispersed droplet phase and a continuous fluid phase. Stabilization of an emulsion is commonly attained by the introduction of interfacially active components, such as surfactants, proteins, or solid particles, that create a steric or thermodynamic barrier to droplet coalescence [35, 27, 19]. As a platform for consumer product formulation, dense emulsions are found in applications ranging from mayonnaise to cosmetic/pharmaceutical creams.

In principle, dense emulsions are not difficult to produce: for example, a simple mayonnaise is made by combining oil, vinegar, and egg yolks in appropriate proportions and blending vigorously [12]. In practice, however, a profitable implementation at industrial scales must be precise, robust, and economical - when addressing these constraints, the true complexities of emulsion processing become apparent. For example, what is the most energy-efficient way to “vigorously blend” two immiscible fluids? Can one devise a combined formulation and processing strategy that reduces the fraction of costly ingredients (oil, egg) while preserving the same stability, taste, and “spreadability” in the final product? In pursuit of such questions, iterations on pilot-scale processing equipment are expensive and time-consuming; therefore, computational and modeling tools have an important role to play, reducing the design-space of interest and accelerating the overall timeline for innovation and deployment of new ideas.

In this work, we will focus on modeling tools that relate processing history to the final droplet size distribution, as might be needed to study “vigorous blending” steps. When formulating dense emulsions, one typically begins from a coarse pre-mix with a population of large droplets, after which complex flows stretch and deform the droplets to induce breakup and establish a final population of smaller droplets [8, 18]. The full details of such a process can be overwhelmingly complex, but here we will outline three existing modeling strategies that provide insights to the relationship between an imposed deformation and the resultant changes in the droplet shape and proclivity to breakup.

Some of the oldest work on the nonlinear rheology of dilute emulsions dates to Taylor [36], who developed a perturbation-expansion approach to model changes in droplet shape at low strain rates,

$Ca \ll 1$, where the Capillary number Ca compares typical viscous stresses and interfacial stresses. Research following this approach has since accounted for higher-order corrections [2, 28] and a broader library of interfacial physics [23, 33]. This vein of research explicitly tracks an approximate representation of the droplet shape evolution, as encoded by a set of symmetric tensors, and the results are indeed useful for understanding the behavior of dilute emulsions at low Capillary numbers. In principle, low- Ca expansions are not suited to describe droplet breakup, but when such theories are extrapolated to $Ca \sim O(1)$ one can find indirect evidence of droplet breakup in terms of a “turning point” in the set of steady flow solutions [2, 33]. In considering dense emulsions, however, the rigor of a perturbation-expansion approach is not feasible, mostly because dense emulsions do not have well-defined flow-fields at the droplet-scale; in heterogeneous materials, one generally expects that individual particles/droplets can experience different local strain histories for the same bulk deformation [6]. Thus, whereas droplet breakup is a deterministic function of strain history in dilute emulsions, it can be viewed as partly stochastic in dense emulsions.

To avoid the complications of explicitly tracking the size and shape of individual droplets, Doi and Ohta (DO) developed a remarkably simple viscoelastic model that achieved closure with only the total droplet stress and the total droplet surface area [7]. The DO model has no conceptual difficulty with dense emulsions or high Ca , and the complex details of droplet breakup and coalescence are simply handled implicitly through the relaxation of stress and surface area. Unfortunately, however, this model has conceptual difficulties with stabilized emulsions, since it is a scale-free model suitable only for systems with neat interfaces where coalescence is not arrested. Additionally, because the DO model avoids tracking the droplet size distribution, it may be less useful in applications where processing objectives are defined in terms of a target droplet size distribution.

Broadly speaking, the above approaches are carefully-derived from well-defined microscopic models, and this rigor naturally gives rise to a more restricted range of application. For a more flexible set of tools with less restricted descriptive power, one can consider more phenomenological models. Neglecting the viscoelasticity of the droplets, for example, one can often infer the shape of a droplet (and its typical time to break) from the instantaneous strain rate [38]. Likewise, the stochasticity of droplet breakup in dense emulsions can be approximated via a Poisson process in a simple first-order rate expression. Dramatic simplifications of this nature still prove insightful for many applications, and the resulting models are simple enough and flexible enough for practical use in complex flow calculations [8, 18]. A closely related simplification strategy beyond the scope of our present interests can also be found in breakage kernels applied in Reynolds-averaged models of turbulent flow. There, the breaking rate is described in terms of the mean turbulent energy dissipation rate [5]. This is an appropriate simplification scheme for Reynolds-averaged models, but not helpful for laminar flows or fully-resolved turbulent flows.

In our view, the principal weakness of existing phenomenological models lies in the loss of viscoelasticity and, more precisely, the loss of an explicit evolution equation pertaining to the droplet shape/stress. The shape of a droplet - as well as its stress and proclivity to breakup - depends not on an instantaneous strain rate but on its entire history of strain. This principle has been clearly demonstrated in the dilute emulsions literature, where Stone et. al. studied the breakup of droplets *after* cessation of flow [34]. To our knowledge, the history-dependence of droplet breakup has yet to be demonstrated directly in experiments on dense emulsions, but here we proceed on the assumption that a connection between droplet breakup and droplet deformation history will exist irrespective of whether the surrounding media is heterogeneous or homogeneous. That being said, it is our view that the details of droplet breakup in dense and dilute emulsions are substantial and will require different mathematical machinery built on different assumptions and abstractions.

Given the abundance of detailed fundamental work on dilute emulsions and the relative dearth of data on droplet breakup dynamics in dense emulsions, it might seem that dilute emulsions present the more natural starting point for model development. However, we argue that for the specific application at hand - coupling rheology and droplet size evolution - it is more natural to begin with dense emulsions. There are many reasons for this, but they all seem to stem from the fact that deterministic breakup events in dilute emulsions present a significant complication for population balance equations, where Poisson-distributed processes are more naturally accommodated. But is it any more reasonable to treat the “stochastic” breakup processes in dense emulsions as Poisson distributed? We think so, but this is really an open question that (to our knowledge) has not even been asked until now. Indeed, absent a useful interpretive modeling framework there has been very little incentive for experiments

that study the statistics and dynamics of droplet breakup in dense emulsions. There are several such approximations and abstractions presented in this report, and it is our hope that these assumptions will not go unchallenged but will instead motivate a focused experimental inquiry.

The outline of our modeling approach is summarized as follows: in keeping with the phenomenological approach, favoring flexibility and simplicity over rigor, we will rely on simple ellipsoidal droplet shapes to interpolate properties of the complex non-ellipsoidal structures encountered in droplet breakup. For a collection of droplets with the same volume, we will compute an average ellipsoidal representation of the droplet shape within that population. When the average droplet shape is sufficiently deformed, breakup proceeds as a Poisson process. The daughter droplets are assumed to be ellipsoidal with a shape consistent with the stress held by the parent droplet. This picture is then extended to all droplet sizes within a given distribution, yielding a set of coupled population balance equations and shape evolution equations, which we call the “shape tensor emulsion population balance” (STEPB) model. Overall, we believe that the STEPB model yields a simple and effective interpolation of the deformation-history-dependent physics relevant to droplet breakup in dense emulsions. Existing models are categorially unable to take on such a challenge, so while there are many aspects of STEPB that remain improvable (e.g. including droplet coalescence and/or surfactant mass transport effects), the progress that we present here should be considered a major step forward.

Briefly, we will summarize two novel ideas that emerge from the STEPB model. First, we will show that conserving stress during droplet breakup creates complex strain-dependent daughter droplet distributions even when individual breakup events are constrained to simple binary splitting. This is possible because the daughter droplets themselves can be sufficiently strained to break again (and again) when the initial imposed strain is large. In our view, this is an important innovation because it is impractical to accommodate history-dependent nuances of the daughter droplet distributions into existing phenomenological models of dense emulsions. Second, in defining an “average” shape for a collection of equally-sized droplets, we provide the first physically-motivated argument for the widely-used log-transformation of a constitutive equation. The mathematical foundations for this transform were developed for computational fluid dynamics (CFD) studies of polymeric materials, as a way of avoiding numerical instabilities [10]. Here, however, we argue that the log-transformation is ideal for handling conserved volume constraints in shape relaxation and shape averaging operations.

The outline of this paper is as follows: In section 2, we outline the bare framework of the STEPB model in terms of coupled equations for momentum balance, droplet size distribution, and droplet shape evolution. In section 3, we continue with more implementation-specific details, relating the ellipsoidal droplet shape tensor to an estimated droplet surface area, stress, and breaking rate. In section 4, we discuss model predictions for monodisperse emulsions in step-shear and outline a strategy for parameterizing the model through a confrontation with experimental data. In section 5, we compare against experimental data for polydisperse emulsions in flows approximating steady simple shear, demonstrating areas of weakness in the current implementation. Finally, section 6 closes the report by summarizing key ideas, results, and directions for future research.

2 Governing Equations

The principle objective of this report is to introduce simplified equations that broadly capture important aspects of the relationship between droplet size distribution and processing history, especially as it pertains to unsteady, complex flow conditions in which the shape of a droplet cannot be reliably inferred from an instantaneous strain rate [34].

To accomplish this, we begin with section 2.1 where we present momentum balance equations, including a discussion on elastic vs capillary stresses and the broader rheological context for which our model has been designed. Then, in section 2.2 we review the general framework of population balance equations (PBE) for describing changes in a droplet size distribution. Finally, we present a viscoelastic constitutive equation for the average droplet shape as a function of droplet size, incorporating the effects of deformation, relaxation, and droplet breakup. Finally, we discuss how the viscous and capillary stresses enter into a momentum balance equation.

This section provides a bare outline of the modeling framework itself, and application-specific details (e.g. the coupling between droplet shape and droplet stress, droplet breakup, etc.) are covered in section 3. In separating the framework from its implementation, we aim to make the model more open to revision and fine-tuning as needed for future research and/or application-specific contexts. The

present implementation as outlined here will be referred to as the “shape tensor emulsion population balance” model, or STEPB. Additional details relevant to numerical solutions of the STEPB model are covered in appendix A.

2.1 Momentum Balance Equations

The rheology of dense suspensions can be classified into at least three distinctive regimes, with the most well-understood regimes being perhaps the least relevant to this work. Thus it is worth taking a moment to identify the relevant rheological context for our present study.

At very low shear rates, the first distinction to consider is whether or not droplets are packed densely enough to create a yield stress material [31]. When the yield stress is below the capillary modulus of a typical droplet (as is especially true for systems just above jamming), droplets remain largely un-deformed and are not susceptible to breakup along the yield surface.

As the shear rate increases, both shear stresses and normal stresses increase in a power-law relation [14], with similar power law scalings for both shear stresses and normal stresses. Here again, viscous stresses are well below the capillary modulus of a typical droplet, and droplet breakup should not be expected.

At higher shear rates, there is evidence that the power law regime transitions to a Newtonian regime [3], but there is comparatively little data for direct observation of said regime. The existence of at least one terminal Newtonian regime is perhaps to be expected, but it is not obvious (1) what factors determine the associated viscosity and (2) whether the indirectly-observed Newtonian regime is indeed the terminal one.

In our work, we consider the third regime, beginning with a Newtonian response, to be the only one relevant to industrial droplet milling processes. The rheological response will be decomposed into two separate contributions: an elastic contribution from droplet capillary stresses, and a viscous response from the constituent Newtonian fluids themselves. For simplicity, we will assume that the effective viscosity for the purely viscous response is both (1) independent of the individual droplet configurations and (2) representative of a “background” viscosity felt by droplets attempting to relax their shape. The estimation and interpretation of such a background viscosity, which we call μ^{eff} , is beyond the scope of our present work but has been considered extensively elsewhere [9, 24], and any of these existing ideas could be appended to our modeling framework in application. We also note that μ^{eff} is distinct from the indirectly-measured Newtonian viscosity measured by Caggioni et. al. [3], since in principle the latter also includes a contribution from the capillary stress response.

Turning now to the momentum balance equations, deformed droplets will exert capillary stresses on the fluid. The total capillary stress tensor $\boldsymbol{\sigma}_T$ enters into the momentum balance equation as:

$$\rho \left[\frac{\partial}{\partial t} \mathbf{u} + \mathbf{u} \cdot \nabla \mathbf{u} \right] = -\nabla P + \rho \mathbf{g} + \nabla \cdot \boldsymbol{\sigma}_T + \mu^{eff} \nabla^2 \mathbf{u} \quad (1)$$

$$\nabla \cdot \mathbf{u} = 0 \quad (2)$$

where \mathbf{u} is the bulk velocity, ρ is the fluid density, P is the pressure, \mathbf{g} is the gravitational field, μ^{eff} is the effective viscosity of the fluid accounting for the total viscous dissipation in both the dispersed and continuous phases. For dense suspensions, we assume that capillary stresses are greater than gravitational forces, such that the suspension exhibits a uniform fluid density and the prospects of droplet settling or gel collapse can be ignored.

The capillary stresses must ensure that the reversible work needed to deform a droplet is equal the change in free energy induced by said deformation - this thermodynamic constraint will be used to specify the relationship between a shape tensor $\boldsymbol{\Theta}$ and the stress tensor $\boldsymbol{\sigma}$ once we have specified a functional form for the droplet free energy $F(\boldsymbol{\Theta})$ in the next section of this work.

2.2 Population Balance Equations

Given a collection of droplets, we define a number density distribution $n(\mathbf{x}, t, v) \delta v$ as the number density of droplets within a small control volume at position \mathbf{x} and time t with droplet volume v in the narrow interval of $v \in [v, v + \delta v]$. For concise notation, the spatial and temporal dependencies of all variables will be notationally suppressed in the equations that follow, and only dependencies on droplet volume v will be shown explicitly.

In the most general expression, the droplet size distribution changes over time due to not only droplet breakup but also processes like advection, diffusion, nucleation, growth, and droplet coalescence [29]:

$$\frac{\partial}{\partial t}n(v) + \nabla \cdot (\mathbf{u}(v)n(v)) = D(v)\nabla^2 n(v) + \dot{n}_B(v) + \dot{n}_C(v) + \dot{n}_N(v) + \dot{n}_G(v) + \dots \quad (3)$$

In equation 3, the second term on the left-hand side (LHS) represents advection with a bulk velocity field $\mathbf{u}(v)$ that may vary with particle size, and the first term on the right-hand side (RHS) represents diffusion with a size-dependent diffusion coefficient $D(v)$. The terms that follow, of which there may be more than those explicitly enumerated here, represent the effect of changes to the droplets themselves: processes like breakup \dot{n}_B , coalescence \dot{n}_C , nucleation \dot{n}_N , and growth \dot{n}_G . In the limited focus of the present work, we are most interested in understanding droplet breakup in unsteady flows - therefore, we will only explicitly consider the breakup term \dot{n}_B . This restricted focus is justifiable when thinking about surfactant-stabilized emulsions with a significant excess of surfactant (e.g. mayonnaise). Likewise, because we are not yet looking at complex flows the advection and diffusion terms will also be suppressed.

Expanding on the breakup term, $\dot{n}_B(v)$ contains two separate terms representing the outflux/influx of droplets with volume v due to (1) the destruction of droplets with size v via breakup and (2) the production of droplets with volume v via the breakup of larger droplets with volume $v' > v$:

$$\dot{n}_B = \dot{n}_{B,\text{in}} + \dot{n}_{B,\text{out}} \quad (4)$$

The outflux of droplets due to breaking $\dot{n}_{B,\text{out}}$ must be proportional to the total number of droplets in the system, $\dot{n}_B(v) \sim n(v)$ with a prefactor $g(v)$ that describes a size-dependent breaking rate:

$$\dot{n}_{B,\text{out}} = -g(v)n(v) \quad (5)$$

For a collection of equally-sized droplets, the rate at which droplets in the group are breaking will depend on the present shape of all individual droplets. Lacking such detailed information, however, one can assume that the overall rate of breaking correlates to an “averaged” measure of the droplet shape - proposed details for such a correlation will be fleshed out in section 3.

The influx term $\dot{n}_{B,\text{in}}$ integrates over all breaking events occurring in droplets of size $v' > v$, weighted by the likelihood $\beta(v, v')$ that a droplet of size v would be produced following breakup of a droplet with size v' :

$$\dot{n}_{B,\text{in}} = \int_v^\infty dv' \beta(v, v') g(v') n(v') \quad (6)$$

The so-called daughter droplet distribution $\beta(v, v')$ can be a major source of complexity in many PBE models of emulsions, since the distribution changes depending on how the droplets were deformed prior to breakup [34]. In our approach, however, we will explicitly track a measure of the droplet shape evolution, and we will allow information about the state of droplet deformation to be inherited by the daughter droplets themselves. Where the first generation of daughter droplets is sufficiently deformed, a second generation of daughter droplets may follow, even in the absence of further deformation. This cascade of breakage eventually terminates, as successive generations of daughter droplets will be less deformed. In our view, the breakage cascade can be used to emulate some aspects of deformation-dependent daughter droplet distributions, though we acknowledge limitations with respect to capturing fine details like satellite droplets.

In all, it is our view that ensuring stress conservation through the breakage process partially alleviates the pressure to construct detailed forms for $\beta(v, v')$, with the details of the breakage kernel now being of secondary importance. Therefore, as a first implementation we will suppose that breakup is always binary and symmetric, $\beta(v, v') = \delta(v - v'/2)$, with every breakup producing just one pair of identical droplets. Many readers may be unconvinced that our assumption of binary breakage is as benign as we claim, given the importance of a carefully-constructed $\beta(v, v')$ in other models for emulsion breakup. For these readers, we have included calculations for a generalization built on a ternary breakup assumption $\beta(v, v') = \delta(v - v'/3)$ in section 4.4, and the differences are found to be small even when all other model parameters are held fixed. Once again, binary and ternary breakage approximations are both too crude to capture fine details like satellite droplets, for example.

With a simplification to binary breakup, the integral in equation 6 collapses and the overall PBE (neglecting all processes except breakup) simplifies to:

$$\frac{\partial}{\partial t} n(v) = -g(v)n(v) + 2g(2v)n(2v) \quad (7)$$

Details of the numerical strategies we have used when solving equation 7 can be found in appendix A. To summarize the appendix contents, we have employed two different schemes depending on the choice of initial condition. Where the droplets are initially monodisperse, we compute the population at discrete droplet sizes corresponding to successive divisions of the original droplet size. Where the droplets are initially polydisperse, we make use of our recently developed “method of the inverse cumulative distribution function”, which is a flexible low-mode discretization strategy that we believe is uniquely suited for solving population balance equations in complex fluids. For further discussion, see appendix A.

2.3 Droplet Configuration Equations

In this section, we will develop equations that describe the evolution of droplet shape in flow. First, section 2.3.1 deals with defining a droplet shape and describing changes to that shape induced by flow, momentarily ignoring capillary forces and population balance dynamics. Next, section 2.3.2 describes the constraints on shape relaxation dynamics (an explicit functional form will be chosen in section 3). Finally, section 2.3.3 considers the average shape evolution for a collection of droplets and the influence of population balance dynamics.

2.3.1 Droplet Shape and Deformation Response

To describe how droplets change shape in response to deformation, we need (1) an expression to define the droplet surface, and (2) an equation to describe how that surface responds to flow. In the most general form, the we can define the droplet surface as a manifold in three-space satisfying $f(\mathbf{r}) = 0$. For motion of the droplet surface, the rigorous approach involves solving momentum balance equations inside/outside of the droplet, coupled by a kinematic boundary condition. Here, we take a more phenomenological approach and assume that droplets deform affinely with a bulk velocity gradient $\boldsymbol{\kappa} = \nabla \mathbf{u}$, less some amount of slip:

$$\frac{\partial}{\partial t} \mathbf{r} = (\boldsymbol{\kappa} - \zeta \mathbf{E}) \cdot \mathbf{r} \quad (8)$$

where $\mathbf{E} = (\boldsymbol{\kappa} + \boldsymbol{\kappa}^T)/2$ is the symmetric portion of the strain field and $\zeta \in [0, 1]$ is the slip parameter. Finite slip may be important when the dispersed phase is significantly more viscous than the continuous phase, for example, increasing the critical shear rate for breakup (c.f. appendix B). For concise notation, we define the effective velocity gradient $\boldsymbol{\kappa}_\zeta = \boldsymbol{\kappa} - \zeta \mathbf{E}$.

Next, we will consider a convenient functional form for the surface manifold equation $f(\mathbf{r}) = 0$. Assuming the droplet has an axis of 180 degree rotational symmetry about its center we can define the droplet shape through a truncated expansion of tensors with increasing rank:

$$f(\mathbf{r}) = -1 + \mathbf{A} : \mathbf{r}\mathbf{r} + \mathbf{B} :: \mathbf{r}\mathbf{r}\mathbf{r}\mathbf{r} + \dots \quad (9)$$

The tensors in this series are all symmetric to any exchange of indices, so a rank-4 tensor needs just 15 unique entries. There are two advantages of describing the droplet surface in this way, namely (1) the opportunity to continuously resolve breakup into isolated droplets with higher-order tensors and (2) the ease of producing evolution equations for shape tensors when using the non-affine deformation rule of equation 8. With regard to the former consideration, note that there can be multiple roots for the intersection of the droplet surface with an orientation vector $\mathbf{n} = \mathbf{r}/|\mathbf{r}|$, which is not possible if the surface is explicitly defined as a function of orientation, $r(\mathbf{n})$.

Here, however, we will restrict ourselves to the assumption of an ellipsoidally shaped droplet, truncating the tensor series at its first term \mathbf{A} . This is a widely used approximation for modeling non-breaking droplets in dilute emulsions [21], but some further discussion is required to interpret its use in dense emulsions and emulsions where droplet breakup occurs.

Regarding dense emulsions, droplet shapes are generally never spherical or ellipsoidal but instead faceted where droplets press together. Here, we suggest that an ellipsoidal approximation is less

intended as a quantitative description of an individual droplet's present shape and should instead be taken as a qualitative description of typical deformations across a collection of droplets.

Regarding droplet breakup, the true process involves a progression of droplet shapes with intermediate structures that cannot be understood as ellipsoidal in any sense. All the same, we argue that a limited set of relevant measures (e.g. surface area and stress) can be effectively interpolated via a superposition of broken (ellipsoidal) and unbroken (ellipsoidal) droplets. We are therefore leveraging droplet breakup to capture both discrete topological transitions and continuous non-ellipsoidal morphological changes. Over-leveraging droplet breakup in this way is likely not appropriate for monodisperse dilute emulsions, where droplet breakup always occurs at discrete moments in time and highly non-ellipsoidal morphologies are possible even without droplet breakup [34]. For dense emulsions, however, we expect that a broader distribution of droplet deformation histories and breakup times makes it impractical or even unnecessary to clearly separate the morphological and topological aspects of the breakup process. For a cartoon schematic of how the ellipsoidal droplet approximation is interpreted for highly distorted droplet shapes very near to breakup, we refer the reader to Figure 2 in section 3.4 and the surrounding discussion.

In this paper, we can not yet provide a complete quantitative assessment for the usefulness of our ellipsoidal approximation in the specific context of dense emulsion droplet breakup - direct observation of individual droplet shapes in dense emulsions under strong flow conditions is a difficult challenge from both experimental and computational approaches, and must be deferred to future work. Without the ability to test this crucial approximation, the goal of this paper is to highlight the promise and potential of the modeling framework that naturally follows.

Continuing with our ellipsoidal droplet approximation, the tensor \mathbf{A} is symmetric, positive definite, rank-2 tensor whose principle eigenvectors identify the axis of an ellipsoid, and whose eigenvalues give the reciprocal square of the corresponding ellipsoid dimensions. The evolution equation for \mathbf{A} can be found by applying a time derivative to equation 9 along the surface $f(r) = 0$:

$$\frac{\partial}{\partial t} \mathbf{A} = -\mathbf{u} \cdot \nabla \mathbf{A} - \boldsymbol{\kappa}_\zeta^T \cdot \mathbf{A} - \mathbf{A} \cdot \boldsymbol{\kappa}_\zeta \quad (10)$$

It is perhaps more useful to frame our shape tensor in terms of its inverse, $\mathbf{C} = \mathbf{A}^{-1}/r_0(v)^2$, so that the principle axis of our shape tensor correspond to the square (as opposed to inverse square) of the axis of the ellipsoid it represents, normalized by the equilibrium (spherical) droplet radius $r_0(v)$. In this case, the evolution equation for \mathbf{C} can be written as:

$$\frac{\partial}{\partial t} \mathbf{C} = -\mathbf{u} \cdot \nabla \mathbf{C} + \mathbf{C} \cdot \boldsymbol{\kappa}_\zeta^T + \boldsymbol{\kappa}_\zeta \cdot \mathbf{C} \quad (11)$$

This is the so-called Gordon-Schowalter derivative commonly used in viscoelastic models of polymeric fluids [16]. As a closing note to this section, the slip parameter ζ can in principle be a function of the shape tensor itself - in studies comparing to experimental results, this could be a useful means of fine-tuning the simplistic picture given here.

2.3.2 Constraints on shape relaxation dynamics

Given an ellipsoidal droplet defined by a shape tensor \mathbf{C} with equilibrium radius r_0 , the volume of the droplet is given by:

$$V = \frac{4}{3}\pi r_0^3 \sqrt{\det(\mathbf{C})} = \frac{4}{3}\pi r_0^3 \quad (12)$$

Note that $\det(\mathbf{C}) \equiv 1$ where the droplet is assumed to be incompressible.

In the absence of flow, we will suppose that droplets relax back to a spherical configuration, $\mathbf{C} = \mathbf{I}$, where \mathbf{I} is the identity tensor. This assumption would fail for dense emulsions with a yield stress, but the yield surface is generally well out-of-frame when emulsions are driven towards droplet breakup (c.f. section 2.1). It is possible to amend our model to hold a finite yield stress by assuming a configuration dependent relaxation time [30], but this is outside the scope of our present interests.

As the droplets relax their shape towards equilibrium, we will first assume that the rate of relaxation for a given droplet depends only on the shape of the droplet in question:

$$\frac{\partial}{\partial t} \mathbf{C} = \dots + \mathbf{R}(\mathbf{C}) \quad (13)$$

Here and elsewhere leading ellipses on the RHS denote terms previously introduced, in this case advection and deformation terms from equation 11.

In seeking a functional form for the relaxation tensor \mathbf{R} , there are two constraints to consider. First, as droplets relax their shape their volume must be conserved at all times, $\det(\mathbf{C}) = 1$, $\partial_t \det(\mathbf{C}) = 0$, yielding the constraint:

$$\mathbf{C}^{-1} : \mathbf{R}(\mathbf{C}) = 0 \quad (14)$$

Second, given a shape-dependent droplet free energy $F(\mathbf{C})$, shape relaxation must decrease the droplet's free energy. Assuming a constant surface tension, this simply becomes:

$$\frac{\delta F}{\delta \mathbf{C}} : \mathbf{R}(\mathbf{C}) \leq 0 \quad (15)$$

Finally, shape relaxation must take place on a time-scale consistent with the balance of viscous and capillary forces in the system. Let us assume that viscous resistance to shape relaxation primarily comes from the medium surrounding the droplet, with viscosity μ^{eff} . Capillary stresses will scale in proportion to the surface tension Γ and inversely with the droplet radius r_0 . If the droplet relaxes its shape on a timescale τ , then viscous stresses will be on the order of μ^{eff}/τ . Balancing viscous and capillary stresses for a single droplet, we find that τ goes as:

$$\frac{1}{\tau} \sim \frac{\Gamma}{\mu^{eff} r_0} \quad (16)$$

and so, considering only the timescale of stress relaxation (and not its dependence on configuration) we find:

$$\mathbf{R}(\mathbf{C}) \sim \frac{1}{\tau} \sim \frac{1}{r_0} \quad (17)$$

For our present purposes, we can define a Capillary number Ca by comparing the imposed strain rate, $\dot{\gamma}$ for simple shear, with the above relaxation time $Ca \equiv \dot{\gamma}\tau$. For $Ca \ll 1$, droplets will be mostly spherical, for $Ca \sim 1$ droplets will be appreciably deformed by flow, and for $Ca \gg 1$ droplets will break apart in flow.

The ideas outlined to this point - an ellipsoidal droplet deforming non-affinely in flow and relaxing in configuration-space along a manifold of conserved volume - are not new [17, 21, 22], but it is important to re-develop these foundations before introducing new ideas in the section that follows.

2.3.3 Shape Averaging and the Log Transform

In the preceding sections, we considered deformation and relaxation for a single ellipsoidal droplet with shape defined by a tensor \mathbf{C} . Here, we will move towards equations that extend these ideas towards a population of droplets with different shapes and sizes, including consideration for population balances and the effects of droplet breakup.

First, we re-interpret $\mathbf{C}(v)$ as a representative average ellipsoidal droplet shape for a droplet of size v . Assuming an underlying population of N droplets with distinct shapes $\mathbf{C}_1, \mathbf{C}_2, \mathbf{C}_3, \dots, \mathbf{C}_N$ and identical volume v , what is a reasonable means of computing a representative average droplet shape? If we require that the volume \bar{v} defined by $\mathbf{C}(v)$ must be equal to the droplet volume in the constituent population, then we cannot define \mathbf{C} as an arithmetic mean. Instead, we must pursue a tensorial analogue of the geometric mean:

$$\ln(\mathbf{C}) = \frac{1}{N} \sum_{i=1}^N \ln(\mathbf{C}_i) \quad (18)$$

taking the trace of equation 18, it is now trivial to show that if $\det(\mathbf{C}_i) = 1$ then $\det(\mathbf{C}) = 1$ and our representative droplet shape has the correct volume. Since the log-transform provides a natural space for shape averaging operations, we will re-cast our shape evolution equation in terms of $\boldsymbol{\Theta}(v) = \ln(\mathbf{C}(v))$. First, considering only the effects of deformation:

$$\frac{\partial}{\partial t} \boldsymbol{\Theta}(v) + \mathbf{u} \cdot \nabla \boldsymbol{\Theta}(v) = \boldsymbol{\Theta}(v) \cdot \boldsymbol{\Omega}^T(v) + \boldsymbol{\Omega}(v) \cdot \boldsymbol{\Theta}(v) + \mathbf{B}(v) + \dots \quad (19)$$

where $\mathbf{\Omega}(v)$ and $\mathbf{B}(v)$ are shape-dependent projections of the rotational and extensional components of the deformation, distinct from the usual symmetric and anti-symmetric portions of the strain rate $\nabla \mathbf{u}$. The details of this log-transformation, including the method of calculation for tensor \mathbf{B} and $\mathbf{\Omega}$ has been worked out elsewhere for the upper convected Maxwell derivative [10], and the generalization to Gordon Schowalter simply requires substituting the non-affine velocity gradient tensor $\boldsymbol{\kappa}_\zeta$ for the affine one $\boldsymbol{\kappa}$. Interestingly, however, our use of the log-transform is the first to invoke a physical as opposed to numerical argument for its usage. Elsewhere, the log-transformation is widely used for its advantage in numerical stability for CFD calculations of viscoelastic fluids [10, 13, 11, 1].

In equation 19, the reader should note that $\mathbf{\Omega}$ and \mathbf{B} are themselves functions of the droplet shape $\mathbf{\Theta}$, so equations 18 and 19 are not entirely self-consistent: the deformation of a log-average droplet shape is now distinct from the log-average of the individual deformed droplet shapes. Here and elsewhere, however, we consider these kinds of pre-averaging approximations as sub-dominant to more significant sources of uncertainty in the model design.

Continuing on to the log-projection of the stress relaxation term, we write:

$$\frac{\partial}{\partial t} \mathbf{\Theta} = \dots + \mathbf{R}_\Theta(\mathbf{\Theta}) \quad (20)$$

where the log-projection of the relaxation tensor $\mathbf{R}_\Theta(\mathbf{\Theta})$ is defined in relation to the relaxation tensor $\mathbf{R}(C)$ in equation 13 by:

$$\mathbf{R}_\Theta(\mathbf{\Theta}) = e^{-\mathbf{\Theta}} \mathbf{R}(e^{\mathbf{\Theta}}) \quad (21)$$

Under the log transformation, the conserved volume constraint is simply represented as $\text{tr}(\mathbf{\Theta}) = 0$, and the equilibrium shape is $\mathbf{\Theta} = \mathbf{0}$. Conceptually, we therefore find it easier to formulate shape relaxation in terms of \mathbf{R}_Θ to avoid the less intuitive constraint of equation 14.

Finally, we proceed to the population balance terms. The total number of droplets in a small control volume δV with droplet size in the interval $v \in [v, v + \delta v]$ is given by $n(v)\delta v\delta V$, and the sum over individual shape tensors within that grouping is given by $n(v)\mathbf{\Theta}(v)\delta v\delta V$. This sum can change over time through advection, deformation, and relaxation as before, but also via the influx/outflux of droplets due to breakup. In the balance equation that follows, we omit the factor of $\delta v\delta V$ from all terms. First, we consider terms relating to advection, deformation, and relaxation:

$$\frac{\partial}{\partial t} (n(v)\mathbf{\Theta}(v)) + \mathbf{u} \cdot \nabla (n(v)\mathbf{\Theta}(v)) = n(v) [\mathbf{\Theta}(v) \cdot \boldsymbol{\Omega}^T(v) + \boldsymbol{\Omega}(v) \cdot \mathbf{\Theta}(v) + \mathbf{B}(v) + \mathbf{R}_\Theta(\mathbf{\Theta})] + \dots \quad (22)$$

Next, we continue to terms pertaining to an influx and outflux of droplets due to breakup. In the most general case, recall from the discussion on equations 5 and 6 that the effects of breakup appear in the number density equation as:

$$\frac{\partial}{\partial t} n(v) = \dots - g(v)n(v) + \int_v^\infty dv' \beta(v, v') g(v') n(v') \quad (23)$$

In the shape evolution equation, every time a droplet departs from or arrives into our reference size interval, its shape is added to or removed from the calculation of an average shape. Hence, in the shape evolution equation we continue from equation 22 and add:

$$\frac{\partial}{\partial t} (n(v)\mathbf{\Theta}(v)) = \dots - g(v)n(v)\mathbf{\Theta}(v) + \int_v^\infty dv' \beta(v, v') \mathbf{\Theta}^{(D)}(v, v') g(v') n(v') \quad (24)$$

where $\mathbf{\Theta}^{(D)}(v, v')$ describes the typical shape of a droplet with volume v that forms upon breakup of a droplet with size $v' > v$. Rules for specifying the shape of daughter droplets will be discussed in section 3. Expanding the time derivative and substituting equation 23 for $\partial_t n(v)$ and assuming $n(v) > 0$ we can simplify. The effects of advection, deformation, and relaxation are given by:

$$\frac{\partial}{\partial t} \mathbf{\Theta}(v) + \mathbf{u} \cdot \nabla \mathbf{\Theta} = \mathbf{\Theta}(v) \cdot \boldsymbol{\Omega}^T(v) + \boldsymbol{\Omega}(v) \cdot \mathbf{\Theta}(v) + \mathbf{B}(v) + \mathbf{R}_\Theta(\mathbf{\Theta}) + \dots \quad (25)$$

and the population balance terms for droplet breakup enter as:

$$\frac{\partial}{\partial t} \mathbf{\Theta}(v) = \dots + \int_v^\infty dv' g(v') \frac{n(v')}{n(v)} \beta(v, v') [\mathbf{\Theta}^{(D)}(v, v') - \mathbf{\Theta}(v)] \quad (26)$$

Since we are primarily interested in the simplest model of breakup, $\beta(v, v') = \delta(v - v'/2)$, equation 26 becomes:

$$\frac{\partial}{\partial t} \Theta(v) = \dots + 2g(2v) \frac{n(2v)}{n(v)} [\Theta^{(D)}(v') - \Theta(v)] \quad (27)$$

Thus we see that an influx of daughter droplets shifts the typical droplet configuration towards that of the incoming daughter droplet population. This is the crucial mechanism by which our framework allows complex daughter droplet distributions to arise from a simple binary breakage rule - the parent droplet's state of deformation is not lost at the moment of breakup but instead transferred to the daughter droplets and distributed across that droplet size interval.

Similar population balance terms can be incorporated into the constitutive equation where there is interest in nucleation, growth, coalescence, etc., but these are beyond the scope of interest for our initial study.

As a final note to this section, the “trick” of transforming to the log-configuration Θ is sensible when the droplets are described in strictly ellipsoidal terms. For a more general case in which droplets are described by a collection of higher-order shape tensors, it is our understanding that this trick is not transferrable. For higher-order tensor generalizations, volume conservation could be handled via an additional isotropic term in the shape evolution equation, modulated by a Lagrange multiplier that constrains shape evolution to a pre-defined manifold of constant volume. For the time being, however, it is our view that there are major technical obstacles to a higher-order tensor implementation (e.g. computing droplet volume and surface area becomes non-trivial) and we find the log-transform approach sufficiently elegant to warrant a departure from a fully future-proof mathematical structure.

3 Details of the Constitutive Equation

In section 2, we worked out a general framework for modeling dense emulsions including population balance equations, droplet shape evolution equations, and momentum balance equations. To this point, however, we have omitted implementation-specific details of the couplings between these equations: how does the droplet shape tensor Θ enter into the capillary stress σ , the breaking rate $g(v)$, and the shape relaxation tensor R_Θ ? And how does the shape of the parent droplet $\Theta(v)$ inform the shape of the daughter droplets $\Theta^{(D)}(v)$ following breakup? In this section, we will sketch a strategy that resolves these questions, but we cannot guarantee the performance of our scheme under any specific engineering application: the details of this section may be subject to revision and improvement as suitable experimental/modeling data is available for confrontation.

To close the STEPB model, we first define a droplet free energy in terms of an estimated surface area. Next, we can describe the associated droplet stress and propose expressions for shape relaxation, checking for positive entropy production and conservation of droplet volume. Finally, we will define daughter droplet shapes and kinetic expressions for droplet breakup.

3.1 Droplet Surface Area Estimation

We will assume that the free energy F of an isolated ellipsoidal droplet is just its surface area, weighted by a surface tension Γ . The surface tension Γ will be assumed to remain constant in time and uniform across the droplet surface, both of which are possible in applications where there is a large excess of surfactant present in solution (e.g. mayonnaise and creams). Future iterations on this modeling framework would be needed to cover systems in which the distribution of surfactant becomes non-trivial.

While there is no closed-form expression for the surface area of an ellipsoid, a suitable estimate - accurate to within about 1% - can be obtained via the Knud-Thomsen approximation [39, 22]:

$$F(\mathbf{C}, r_0) = 4\pi r_0^2 \Gamma \left(\frac{1}{3} I_2(\mathbf{C}^{p/2}) \right)^{1/p} \quad (28)$$

$$I_2(\mathbf{X}) = \frac{1}{2} (\text{tr}(\mathbf{X})^2 - \text{tr}(\mathbf{X}^2)) \quad (29)$$

where I_2 is the second frame invariant and the value $p = 1.6$ optimizes the approximation across a wide space of ellipsoids. A similar estimation of surface area was previously made for highly faceted

emulsions, where $p = 2$ was considered more appropriate [15]. We will continue to use $p = 1.6$ for the remainder of this report to remain internally consistent with our ellipsoidal approximation of droplet shapes, but within this range we do not consider the choice of p to be extremely important compared to other assumptions and approximations within the model.

To compute the total free energy F_T of a collection of droplets with log-averaged shape tensor Θ , we rely on a pre-averaging approximation - within a given volume range $v \in [v, v + \delta v]$, we assume that the surface area of the average droplet shape is the same as the average surface area of the underlying droplet shapes. Summing over the free energy from all possible droplet sizes, we obtain:

$$F_T = \int_0^\infty dv n(v) F(e^{\Theta(v)}, r_0(v)) \quad (30)$$

This pre-averaging approximation works best when the droplet shape at any size v is narrowly distributed. For more broadly dispersed droplet shape distributions, our pre-averaging approximation will underestimate the free energy. Unfortunately, in our view it is not possible to improve on this preaveraging approximation without compromising the overall simplicity and computational cost of the framework outlined in section 2.

3.2 Droplet Stress

The reversible work needed to deform a droplet must be equal to the change in free energy associated with the change in droplet shape [16, 32]. Since we know that the shape tensor \mathbf{C} is deformed by a Gordon-Schowalter derivative and the free energy in equation 28 is defined explicitly in terms of that same shape tensor, it is possible to define the droplet's elastic stress $\sigma(\mathbf{C})$ by which the fluid resists deformation [16]:

$$\sigma(\mathbf{C}, v) = 2(1 - \zeta) \mathbf{C} \cdot \frac{\delta F}{\delta \mathbf{C}} \quad (31)$$

Evaluating the derivative on F using equation 28, this becomes:

$$\sigma(\mathbf{C}, v) = n(v) v \left(\frac{\Gamma}{r_0(v)} \right) (1 - \zeta) (I_2(\mathbf{C}^{p/2})^{(1/p-1)} (\text{tr}(\mathbf{C}^{p/2}) \mathbf{C}^{p/2} - \mathbf{C}^p)) \quad (32)$$

Note that the capillary stresses are proportional to a modulus $G_0 = \Gamma/r_0$ that increases with surface tension and decreases with droplet radius. To compute the total stress in a collection of droplets, we once again use our pre-averaging approximation and assume that the average stress from a collection of equally-sized droplets is the same as the stress from a droplet with average shape:

$$\sigma_T = \int_0^\infty dv \sigma(e^{\Theta(v)}, r_0(v)) \quad (33)$$

3.3 Shape Relaxation

As discussed in section 2.3.2, the shape relaxation tensor $\mathbf{R}_\Theta(\Theta)$ must be traceless to conserve droplet volume, $\text{tr}(\mathbf{R}_\Theta) = 0$, and it must also ensure positive entropy production to be thermodynamically consistent. The simplest means of satisfying these constraints is to assume that stress relaxation is linear in Θ :

$$\frac{\partial}{\partial t} \Theta(v) = \dots - \frac{1}{\tau(v)} \Theta + \dots \quad (34)$$

where the relaxation time $\tau(v)$ depends on the droplet volume and is found by balancing elastic and viscous forces during the shape relaxation process, as discussed in section 2.3.2. In particular, the relaxation time $\tau(v)$ scales inversely with the droplet's equilibrium radius, $\tau(v) \sim v^{-1/3}$. Projecting this expression for shape relaxation back to the shape tensor $\mathbf{C} = e^\Theta$, this becomes:

$$\frac{\partial}{\partial t} \mathbf{C} = \dots - \frac{1}{\tau(v)} \mathbf{C} \cdot \ln \mathbf{C} \quad (35)$$

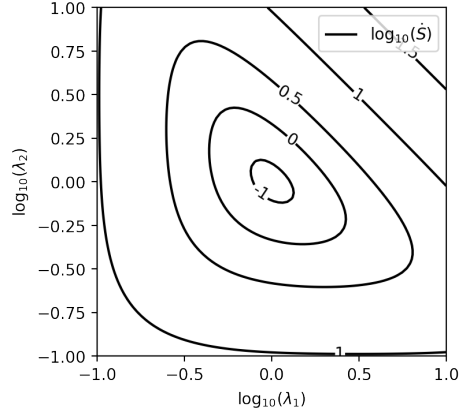


Figure 1: Demonstrating positive entropy production per equation 36 over a wide range of possible droplet shapes, as defined in terms of the two independent eigenvalues λ_1 and λ_2 of the droplet shape tensor \mathbf{C} . Note that we plot contours of $\log_{10}(\dot{S})$ for more even spacing, so contours with negative labels still represent positive entropy production. Per-particle entropy production has assumed units of $v\mu^{eff}/\tau^2(v)$ in this figure.

In the figure below, we provide a contour plot of the per-droplet rate of entropy production \dot{S} (in units of $v\mu^{eff}/\tau^2(v)$) as a function of the two independent eigenvalues, λ_1 and λ_2 of a configuration tensor \mathbf{C} . Note that the third eigenvalue λ_3 is constrained by $\det(\mathbf{C}) = \lambda_1\lambda_2\lambda_3 = 1$.

$$\dot{S}(\mathbf{C}) = -\frac{\partial F}{\partial \mathbf{C}} : \mathbf{R}(\mathbf{C}) = \frac{1}{\tau} \frac{\partial F}{\partial \mathbf{C}} : (\mathbf{C} \cdot \ln(\mathbf{C})) \quad (36)$$

In figure 1, we see that entropy production goes to zero when the droplet shape is at equilibrium, $\mathbf{C} = \mathbf{I}$, and it is strictly positive for droplets deformed from equilibrium. We have also explored a wider range of simple expressions for $\mathbf{R}(\mathbf{C})$ and it does not appear to be difficult to construct relaxation tensors that satisfy the constraints of equations 14 - 17. In our experience, any reasonably constructed relaxation tensor that conserves droplet volume (the easier constraint to design around) tends to also show positive entropy production for the free energy as defined in equation 28.

To close this section, we note that a considerable body of work already exists for describing the shape evolution of ellipsoidal droplets in *dilute emulsions*, complete with comparisons to experimental data [17, 21, 22]. One might reasonably argue that our model could be immediately improved by applying the tried-and-tested shape relaxation tensors employed therein, but we defer such an approach for the time being for two reasons: (1) what is true about shape relaxation in dilute emulsions may not be true for dense emulsions, since the limits of our “effective medium approximation” are not yet established from experiments, and (2) the shape relaxation tensor is not necessarily the main deficiency of the overall modeling framework, and corrections on \mathbf{R}_Θ will make the overall modeling framework more complex but not necessarily better given the limitations that persist elsewhere.

3.4 Daughter Droplet Shapes

The conditions under which droplets can break apart will be covered in section 3.5, but we will briefly preempt that discussion to think about the shape of the daughter droplets left behind after droplet breakup takes place. In keeping with the framework outlined in section 2.3.3, we will assume that daughter droplets are purely ellipsoidal in their shape.

Here, we consider the following scenario: prior to breaking, a parent droplet with volume v has shape tensors \mathbf{C} and $\Theta = \ln(\mathbf{C})$, and the breakup process produces two identical daughter droplets with volumes $v/2$ and shape tensors $\mathbf{C}^{(D)}$ and $\Theta^{(D)} = \ln(\mathbf{C}^{(D)})$. Ideally, we would like to specify the droplet shape such that there is perfect continuity across the breaking event - the daughter droplet would have the same surface area and the same stress as the parent droplets, for example. Unfortunately, however, it is not possible to ensure continuity across both these measures.

An ellipsoid is specified through six independent pieces of information: three to define the length of each axis, and three more to orient it in space. If we assign the orientation of the daughter droplet

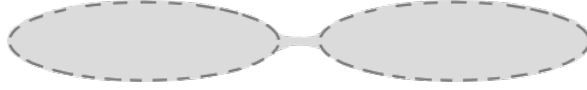


Figure 2: Cartoon representation for our interpretation of the ellipsoidal droplet approximation as it pertains to assigning daughter droplet shapes. The above droplet is technically unbroken - topologically speaking it is a single non-ellipsoidal manifold, but many of its physical properties (stress, surface area, etc) can be reasonably captured via a pair of ellipsoids in this case. Daughter droplet shapes are defined such that stress relaxes continuously through the whole breakup process.

to that of the parent droplet, then we need three additional constraints to specify the daughter droplet shape. This can be achieved by matching the principle components of the parent/daughter droplet's deviatoric stress tensors:

$$\boldsymbol{\sigma}(\mathbf{C}^{(D)}, v/2) + \Lambda I = \frac{1}{2} \boldsymbol{\sigma}(\mathbf{C}, v) \quad (37)$$

Specifying the daughter droplet shape in this way, it is no longer possible to constrain the change in surface area that occurs through breaking. In fact, we find that conserving droplet stress always leads to an increase in droplet surface area following breakup, in violation of basic thermodynamic principles. Conversely, if we constrain the daughter droplet shapes to a manifold of specified total surface area, then in our view there is no clear basis to specify three axis of an ellipsoid with just two additional pieces of information.

At this point, it is helpful to remember that droplet breakup is, in reality, defined by a discrete topological transition (from one closed manifold to two or more) that takes place in the course of droplet shape evolution. With a higher-order tensor representation of the droplet shape, it would be possible to resolve such a transition explicitly, with all the relevant physics encoded in shape relaxation tensors like $\mathbf{R}(\mathbf{C})$. Having constrained ourselves to ellipsoidal projections of droplet shape, however, we have lost the capacity to resolve topological transitions explicitly, and instead must resolve them implicitly. Thus, we argue that inquiries on thermodynamic consistency must treat shape relaxation and droplet breakup as joint processes, assessing only the net entropy production of the two processes combined. In section 4.3 we will show that if the kinetics for breakup and shape relaxation are bound to similar timescales, the net entropy production from shape relaxation will indeed be positive.

To close this section, some readers may find our choice to conserve droplet stress across breakup surprising: after all, surely there must be some stress relief associated with the breakup process? Here, we remind the reader that we are effectively using the daughter droplets and parent droplets together as a means of interpolating properties of the intermediate states that lead to breakup - some portion of stress relaxation in the daughter droplet distribution is effectively serving as a proxy for fast-relaxing capillary modes that would exist in a higher-order representation of the parent droplet shape. Therefore, conserving stress at the moment of breakup does not preclude an indirect benefit to stress relaxation across the whole breakup process. A similar coupling between stress relaxation and breakup has previously been described for polymeric materials [4, 26].

This same idea can be communicated graphically in the cartoon of Figure 2: topologically speaking there is only one droplet, but in many respects its shape is better described as two ellipsoids arranged head-to-tail. To choose the pair of ellipses that best captures the contorted shape of the parent droplet, we suggest matching the capillary stresses. This assumption is physically grounded in the overall continuity of the breakup process - the stress relaxation attributed to breakup is realized through a gradual shape relaxation and not an instantaneous topological transformation.

3.5 Breakup Dynamics

In dilute emulsions, droplet breakup is deterministic based on the bulk strain history. For dense suspensions, however, deformation at the scale of individual droplets is less predictable - for the same bulk deformation, individual droplets can experience different deformations and thus breakup times become more broadly distributed.

Working from our ellipsoidal approximation of droplet shape, there are two natural ways that one might represent the breaking rate $g(v)$ in equation 7. First, as might be appropriate for dilute emulsions, we could say that there exists a bounding manifold in shape-space $f(\boldsymbol{\Theta}) = 0$ that defines

a “breaking surface”. Droplets within the envelope of this manifold remain cohesive but split spontaneously upon reaching the breaking surface leading to a breaking rate that is delta-distributed in time:

$$g(v) = \delta(f(\Theta(v))) \quad (38)$$

Even for dilute emulsions, however, this expression is problematic when the shape is constrained to be ellipsoidal. For higher-order descriptions of the droplet shape, the key property of the breaking surface is that it marks the boundary of a topological transition, and no such boundary can be marked on the space of ellipsoids.

For dense emulsions, delta-distributed breaking rates are also unacceptable on a more fundamental level - one would prefer a distribution of breaking times to reflect the distribution of droplet-scale strain histories. The simplest possible approximation is to assume that for a given average droplet shape Θ , breaking times are Poisson-distributed (memoryless) with a driving force towards breakup that can be inferred from the average shape alone via some function $h(\Theta, v)$. We further assume that the timescale for breakup is tied to the timescale for shape relaxation, with some $O(1)$ proportionality factor α :

$$g(v) = \frac{\alpha}{\tau} h(\Theta, v) \quad (39)$$

Following our discussion in section 3.4, we note that the prefactor α will have an important role to play with respect to guaranteeing the thermodynamic consistency of the joint breaking/shape relaxation process. For simplicity, we will assume that the driving force for breakup is proportional to the difference in surface area between the current state (deformed ellipsoidal droplet) and a hypothetical end-state of the shape relaxation/breakup process (two spherical droplets):

$$F_{brk}(r_0(v)) = 2F(\mathbf{I}, r_0(v/2)) \quad (40)$$

$$h(\Theta, v) = \begin{cases} 0 & \text{if } F(e^\Theta, r_0(v)) \leq F_{brk}(r_0(v)) \\ F(e^\Theta, r_0(v))/F_{brk}(r_0(v)) - 1 & \text{if } F(e^\Theta, r_0(v)) > F_{brk}(r_0(v)) \end{cases} \quad (41)$$

Recall again that the shape tensors \mathbf{C} and Θ are related by $\mathbf{C} = e^\Theta$, and $F(\mathbf{C}, r_0)$ is the free energy (proportional to surface area) of a droplet with equilibrium radius r_0 and ellipsoidal shape defined by \mathbf{C} . This simplistic picture of $h(\Theta, v)$ qualitatively captures an increasing proclivity to breakup with increasing extent of deformation, but it has at least one major weakness in that it takes no consideration for the type of deformation being applied. For example, the same change in surface area could be achieved with either a prolate or oblate spheroid, but the former generally is far more susceptible to breakup.

More general rate expressions (e.g. including memory functions) are possible but in our view difficult to parameterize in a simple but compelling way. As such, we feel that a Poisson-approximation of breaking time distributions provides the most appropriate balance of simplicity and insight for our present interests.

This concludes our presentation for the governing equations of the STEPB model.

4 A Path to Parameterization: Sample Calculations for Monodisperse Systems

Having finalized the details of STEPB in section 3, here we will provide a first set of calculations and discuss a path towards parameterizing the model and testing its predictions on the basis of comparisons to experimental data. As mentioned in the introduction, for the purposes of quantitatively testing our model there is presently an insufficient body of experimental work on time-dependent droplet breakup in stabilized dense emulsions. Therefore, we will instead use this opportunity to propose a new design of experiments that could challenge the predictions of STEPB and determine its usefulness as a framework for modeling dense emulsions.

Droplet breakup in monodisperse dense emulsions following a step shear deformation poses a number of conceptual challenges for existing models [8, 18, 7]. In step shear, the processes of deformation

and relaxation/breakup do not occur concurrently but sequentially. This separation of deformation and breakup is important for describing processes at high Deborah number, where the Deborah number De compares the timescale for *changes in strain rate* against the droplet's natural relaxation time τ . Only viscoelastic models are capable of appropriately separating deformation and breakup, and to our knowledge the STEPB model is the first to include the requisite coupling between the population balance equations and the droplet shape evolution equations.

In the absence of experimental data, we will briefly discuss the an expected outcomes of the proposed step-deformation experiment - this will guide our interpretation of the model predictions that follow. First, we expect that for small deformations, droplets will relax back to an isotropic shape without breaking, leading to no net change in the droplet size distribution. Above some critical deformation, a fraction (not all) of the droplets will begin to break. This is distinct from what should be expected in dilute emulsions, where outcomes are strictly determined. Finally, with increasing initial deformation more and more of the droplets will break into smaller and smaller fragments. These expected outcomes seem reasonable, but they should not stand unchallenged - it is our view that studying the dynamics of droplet breakup in dense emulsions should be just as productive today as studying the dynamics of droplet breakup in dilute emulsions was four decades ago.

As a further motivation to consider step-shear calculations, step-shear provides a self-contained parameterization of STEPB where complete experimental data is available. As currently formulated, the STEPB model can be fully specified through an initial droplet size distribution plus four additional parameters, namely the surface tension Γ , a slip parameter ζ , a reference droplet relaxation time τ , and a kinetic prefactor α governing droplet breakup dynamics. The viscosity μ^{eff} is omitted from this list, since it obviated by the assumed relation $\mu^{eff} \sim \Gamma\tau/r_0$. Our parameter list also lacks explicit reference to the viscosity ratio of the component Newtonian fluids - the viscosity ratio should end up modulating the slip parameter ζ , as is extensively documented in the literature on dilute emulsions [21]. The viscosity ratio should also modulate other model parameters, including the kinetic prefactor α and the precise relationship between μ^{eff} and τ . At present, there is insufficient data on droplet relaxation/breakup in dense emulsions to properly codify an explicit dependence on the viscosity ratio, so these details must be deferred to future work.

In section 4.1, we will show that the surface tension Γ and slip parameter ζ can be found through the linear and nonlinear elasticity of an emulsion. In section 4.2, we will show that a relaxation time τ is evident through the stress relaxation dynamics. In section 4.3, we will show that the kinetic prefactor α changes both the final particle size distribution and the stress relaxation kinetics. Finally, in section 4.4 we will explore trends for strain-dependent daughter droplet distributions that emerge in the STEPB model.

The calculations that follow consider a monodisperse dense emulsion with droplet volume v_0 and total volume fraction ϕ . Note that the total volume fraction is related to the number density distribution by $\phi = \int_0^\infty n(v)v dv$, so that $n(v) = \delta(v - v_0)\phi/v_0$ for the case of monodisperse emulsions.

For additional details on the numerical methods of solution, we refer the reader to appendix A.

4.1 Nonlinear Elasticity: Modulus and 'slip' parameter

The surface tension of a monodisperse dense suspension can be indirectly measured through its linear elastic response to deformation, and the propensity to 'slip' can be similarly inferred from a nonlinear elastic response. Here, we will consider predictions for the linear and nonlinear elasticity with respect to step shear, since shear deformations are typically easier to realize in experiments.

In Figure 3, we plot the dimensionless shear stress $\sigma_{xy}/\phi G_0$ as a function of the shear strain amplitude γ . First, we note that the linear elastic response has a modulus $G = G_0 p/2$, where $p = 1.6$ in the Knud-Thomsen approximation. Strain-softening in the absence of slip occurs at high strain where changes in droplet surface area become linear (as opposed to quadratic) in the applied strain. Inclusion of a slip parameter ζ enhances strain softening in the nonlinear elastic response, as droplets begin rotating away from the axis of extension without stretching. At sufficiently large strains, even small amounts of 'slip' can lead to dramatic changes and 'tumbling' when droplets over-rotate and shear stress becomes an oscillatory function of strain amplitude.

Where experimental data is available, the linear elastic response provides a means of estimating the surface tension Γ , via $\Gamma = 2Gr_0/p$. The nonlinear elastic response can also inform the description of 'slip' effects wherever $\zeta = 0$ under-predicts strain softening at large strains. The choice of ζ will influence the critical capillary number in steady shear flow (c.f. section 5), and ideally correcting for

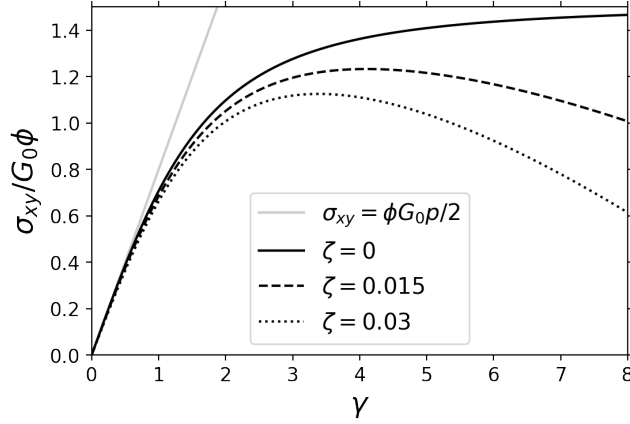


Figure 3: STEPB model predictions for the linear and nonlinear elasticity of a monodisperse dense emulsion under step shear deformation. The linear elastic response $\sigma_{xy} = \phi G_0 p/2$ provides a means of estimating the surface tension via $G_0 = \Gamma/r_0$. The nonlinear elastic response provides a means of further fine-tuning the model to account for a slip parameter ζ as and when such corrections are necessary.

slip in the elastic response should provide a more accurate prediction of the critical capillary response in steady shear - where this is not the case, however, it must be recognized that the way we describe droplet deformation bypasses the underlying hydrodynamics problem and is thus subject to error. In practice, therefore, it may often be more useful to use ζ as a means of tuning the critical capillary number (c.f. appendix B) rather than the nonlinear elastic response to step deformation.

For completeness, figure 4 gives STEPB model calculations of the first and second normal stress differences in step shear for $\zeta = 0$. The results are similar to models discussed elsewhere in the literature [15], in that the first and second normal stress differences are comparable in magnitude but opposite in sign, and normal stresses increase linearly with strain for $\gamma \gg 1$.

Unless stated otherwise, all calculations that follow will assume $\zeta = 0$.

4.2 Medium strains without breakup: linear relaxation time

At large strains, droplets will be prone to breakup, but small strains in dense suspensions will often have a yield stress that precludes observation of a shape relaxation timescale. Therefore, intermediate strains may be most useful for parameterizing the STEPB model's shape relaxation time τ . However, because the stress tensor σ_T and relaxation tensor R_Θ are not linearly related to one another, there is no a-priori guarantee that stress relaxation following nonlinear deformations will yield a single easily measured relaxation time. If nonlinearities dominate stress relaxation at early times for intermediate strain deformations, then it may be difficult to uniquely parameterize the model, since droplet breakage is a confounding source for nonlinearity in the overall stress relaxation. In the absence of experimental data for comparison, this section will simply test whether such nonlinearities dominate stress relaxation in the STEPB model, since this is a necessary (albeit not sufficient) condition for the success of our proposed parameterization strategy.

Here, we consider predictions of the STEPB model for strain $\gamma = 1$. This strain is below our proposed critical strain for breakup $\gamma = 1.5$ (c.f. section 3.5), but well above a typical yield strain for weakly jammed dense emulsions, $\gamma \sim 0.03$ [31]. The predictions are shown in figure 5, wherein it is evident that stress relaxation is effectively linear, with relaxation time τ , over the entire time interval of interest. Where a yield surface is present, the linear relaxation process will be interrupted as the droplets approach a stable isostatic configuration. Figure 5 also shows that stress relaxation is directly correlated to a decrease in the total droplet surface area Ω_T relative to the pre-strained surface area Ω_T^{eq} .

Where the relaxation time τ , the surface tension Γ , and the monodisperse droplet size r_0 can all be measured independently, it is possible to infer an estimate of the effective emulsion viscosity μ^{eff} indirectly, via $\mu^{eff} = \Gamma\tau/r_0$. This estimate of μ^{eff} can be further tested through steady shear

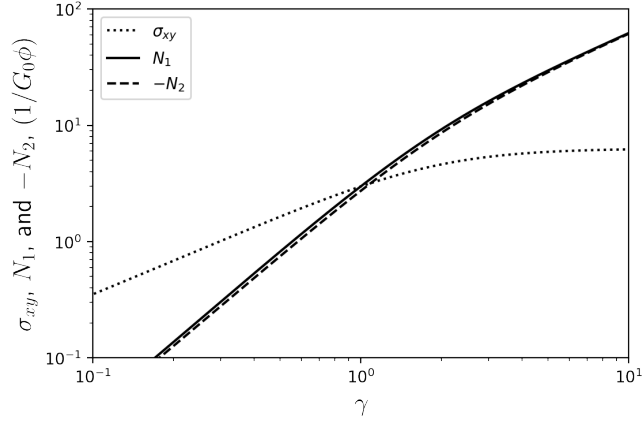


Figure 4: Comparing the normal stress differences N_1 and $-N_2$ with the shear stress σ_{xy} over a range of strain amplitudes γ . Across all strain amplitudes, the first and second normal stress differences are comparable in scale but opposite in sign. At low strains, normal stresses increase quadratically, while at high strains they increase linearly.

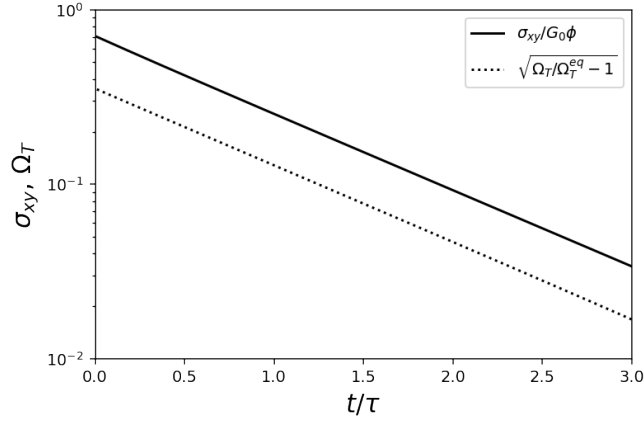


Figure 5: Predictions for stress relaxation following a medium-amplitude deformation, where the capillary stresses are more reliably measured and droplet breakup is not yet taking place. In the STEPB model, the recovery of both stress and surface area can be described as single-exponential processes on the time interval considered above.

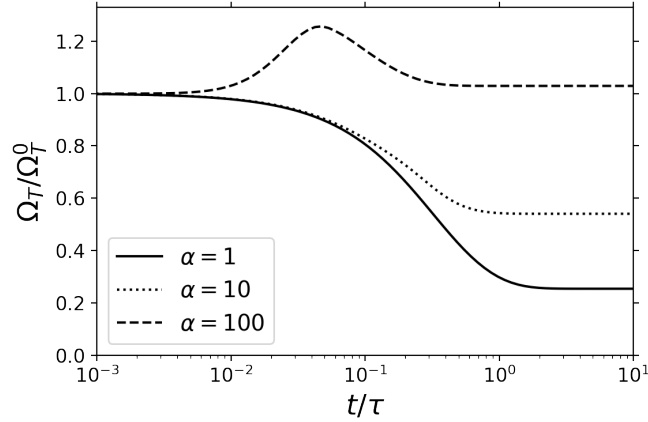


Figure 6: Predictions of the STEPB model with $\zeta = 0$ for total surface area during the process of relaxation from an initial step strain of $\gamma = 10$. The kinetic prefactor to the breaking rate, α , controls how quickly breaking occurs relative to shape relaxation. Larger values of α allow more breaking events to occur, and leading to a steady state with smaller average droplet size and higher overall surface area. Excessively large values of α are problematic, however, leading to a transient increase in the total surface area. The source of this non-physical behavior, is discussed in the main text.

measurements, provided (1) stresses are well above the yield stress and well below $Ca \sim 1$ and (2) the viscous contribution to the stress is appropriately isolated from the capillary stress contribution.

4.3 Large strains with breakup: breakup kinetics

Continuing to large strains, here we explore both implicit and explicit signatures of droplet breakup in the STEPB model. Implicit signatures of droplet breakup can be found by observing stress relaxation, whereas explicit signatures of droplet breakup are evident through direct measurement of a droplet size distribution. Assuming parameters Γ, ζ , and τ are already known through independent means, these measurements can help assign the kinetic prefactor to breakup, α , which controls the relative timescales for shape relaxation and droplet breakup. Because droplet surface area increases discontinuously for individual breakup events, we first need to check that our choice of α maintains a thermodynamically consistent joint description of relaxation/breakup.

Here, we evaluate the total surface area Ω_T normalized by the initial surface area after deformation Ω_T^0 following a step-strain of $\gamma = 10$. Predictions are shown for $\alpha = 1, 10, 100$ in figure 6. For $\alpha = 1, 10$ there are no issues - the total surface area is always decreasing in time, and increasing α allows droplets to break faster and preserve more of the extra surface area created during the initial deformation. However, for $\alpha = 100$ droplets are able to break much faster than they can relax and since each successive break leads to an increase in surface area (c.f. section 3.4) we observe a non-physical transient increase in the total surface area.

Because surface area must continually decrease during relaxation/breakup, large values of α lead to a model that is thermodynamically inconsistent. However, in constructing the STEPB model, α was never intended to take on any arbitrary value - it was always intended as a means of modulating the relationship between the physically connected processes of shape relaxation and droplet breakup, taking on a value $\alpha \sim O(1)$. Absent experimental data for a direct comparison, for convenience we will use $\alpha = 10$ to amplify the effects of breakage while still remaining safely in the space of thermodynamically consistent predictions. This choice does not necessarily endorse $\alpha = 10$ as a realistic value, and in application varying α will be an important handle for matching experimental data.

As a complement to Figure 6, we also show in figure 7 the final droplet size distribution in terms of a cumulative distribution function (CDF), $\Phi(v) = 1/\phi \int_0^v n(v)v dv$. Figure 7 covers the same initial strain $\gamma = 10$ and the same values of $\alpha = 1, 10, 100$. With increasing α droplets are better able to break while they remain deformed, leading to smaller droplet sizes in the final distribution. Note that the CDF is a stepwise function because the droplet size distribution is described through a series of delta-peaks in this case.

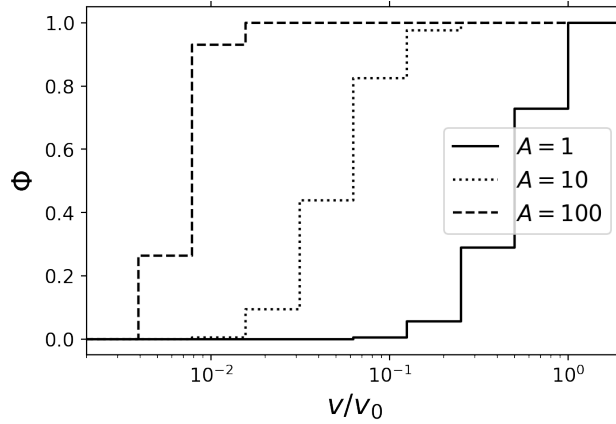


Figure 7: The final daughter droplet size distribution following an initial strain of $\gamma = 10$ for $\alpha = 1, 10, 100$, $\zeta = 0$. This figure provides complementary information to figure 6.

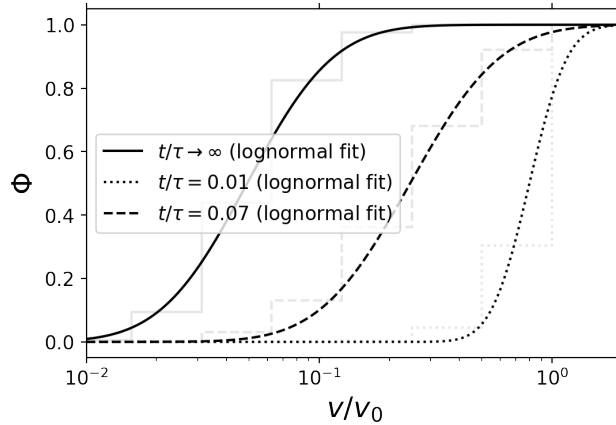


Figure 8: For an initial strain of $\gamma = 10$ and a kinetic prefactor $\alpha = 10$ (see figures 6 and 7), we show the time-evolution of the cumulative distribution function (CDF) on the droplet size distribution, $\Phi(v) = 1/\phi \int_0^v n(v)vdv$. As droplets break apart, the typical droplet size decreases and the variance in the distribution increases.

In reality, there is no reason to expect such step-wise changes from experimental observations: the delta-distributed size distribution is a combined consequence of assuming a delta-distributed initial condition and strict binary, symmetric breaking events. However, the broad trends underlying the discrete distributions may in fact be represented in experiments. In Figure 8, we show that the broad trends reflected in the step-wise daughter droplet distribution can be reasonably approximated by constructing a log-normal distribution fit to the same mean and variance. At time-slices $t/\tau = 0.01, 0.07, \infty$, we show the discrete CDF (light grey lines) and its smooth approximation (black lines).

Figure 8 is interesting to consider, but unfortunately it may generally be difficult to directly measure a droplet size distribution at intermediate relaxation times. Fortunately, however, signatures of droplet breakup are also evident during stress relaxation. As droplets break apart, the smaller daughter droplets are able to relax their shape faster than the original parent droplets. In figure 9, we confirm that the faster shape relaxation likewise translates to faster stress relaxation, which is more readily measured than a droplet size distribution.

As a counterpart to figure 9, increasing strain amplitude can have a similar effect to increasing α , in that it produces faster breakup and smaller final droplet sizes. Therefore, in figure 10 we show the influence of strain amplitude on stress relaxation for fixed $\alpha = 10$ at strains $\gamma = 1, 5, 20$. For sufficiently small strains $\gamma = 1$, stress relaxation is effectively linear as previously seen in figure 5. For larger strains, stress relaxation quickly becomes linear but with a characteristic relaxation time

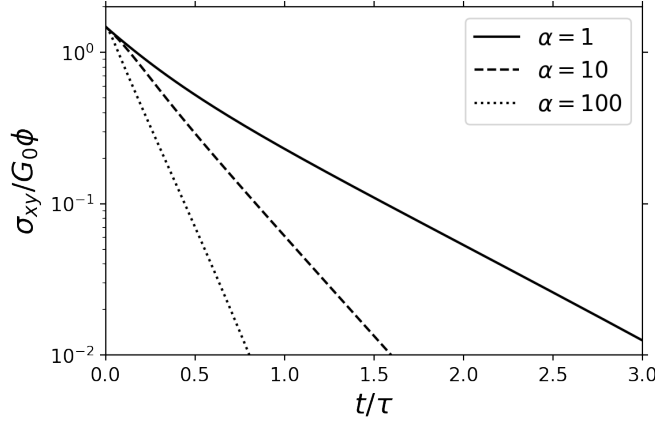


Figure 9: Predictions of the STEPB model for stress relaxation following a strain of $\gamma = 10$ with varying kinetic prefactor to breakup $\alpha = 1, 10, 100$ and $\zeta = 0$. Accelerating droplet breakup moves the droplet stress to faster-relaxing structures, which in turn leads to faster stress relaxation dynamics. By comparing stress relaxation kinetics at low strains (c.f. figure 5) and high strains, it should be possible to infer an appropriate choice of α .

that decreases with increasing strain amplitude, since the typical droplet size decreases with increasing strain amplitude.

4.4 Strain-dependence in final daughter-droplet distribution

To close this section, we will discuss the broad trends that emerge in STEPB when exploring the influence of initial strain on the final daughter droplet distribution. Because changes in the size distribution are reasonably approximated by a log-normal distribution (c.f. figure 8), we will report these results in terms of changes to the mean droplet size \bar{v}/v_0 and the relative standard deviation $\bar{\sigma} = \langle v - \bar{v} \rangle^{1/2}/v_0$. In figure 11, we see that for increasing initial strain, the final daughter droplet distribution is characterized by increasing polydispersity and decreasing average droplet size.

Although experimental data is not yet available for comparison, we expect that the trends reflected in figure 11 are physically reasonable and we look forward to an eventual confrontation with experimental data as and when such data becomes available. Here, we once again remind the reader that our predictions for strain-dependent daughter droplet distributions come from a very simple set of rules governing the breakup process. There is ample room for refinement as supported by data and required by application.

To close this section, we want to discuss the influence of the binary breakage approximation, which is perhaps the most easily identifiable weakness of the STEPB model. While it is possible to generalize the STEPB model to consider arbitrary daughter droplet distributions, here we will show that the predictions given in figure 11 are relatively insulated against changes to the breakup kernel that would ordinarily be considered significant, even while all other model parameters are held fixed. For example, the assumptions and approximations of the STEPB model can easily be revised to ternary breakup, where each droplet breaks apart into three identical daughter droplets with the same deviatoric stress. As shown in figure 12, the move from binary to ternary breakup slightly increases the critical strain, as the critical strain reflects a state where the broken droplets (if spherical) have a lower surface area than the stretched droplet. At higher strains, the final mean size of a daughter droplet \bar{v}/v_0 is roughly independent of the binary/ternary approximation, but the variance in the distribution is slightly higher for ternary breakup.

Thus, while fine-tuning of the daughter droplet distribution will have some effect on STEPB model predictions, such adjustments necessarily introduce adjustable parameters at a cost to the model's simplicity. As presently formulated for binary breakup, we feel that STEPB strikes a good balance between physical detail and conceptual simplicity suitable for many applications.

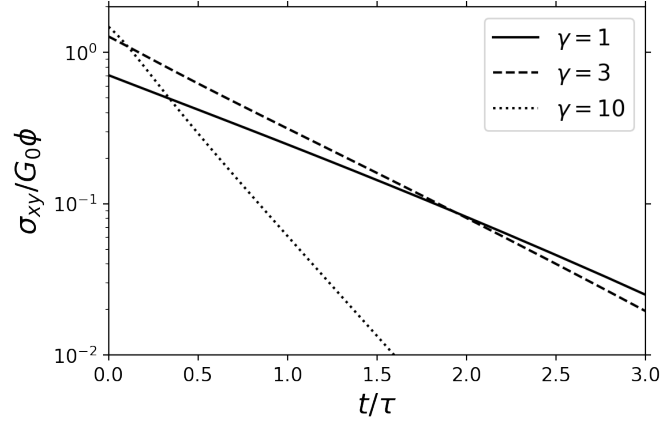


Figure 10: STEPB model predictions for stress relaxation after strains of amplitude $\gamma = 1, 3, 10$. The initial stress increases with increasing strain, but after a short time the droplets break apart and the resultant daughter droplets are able to relax their stress more quickly, which translates to a lower overall stress after a short time.

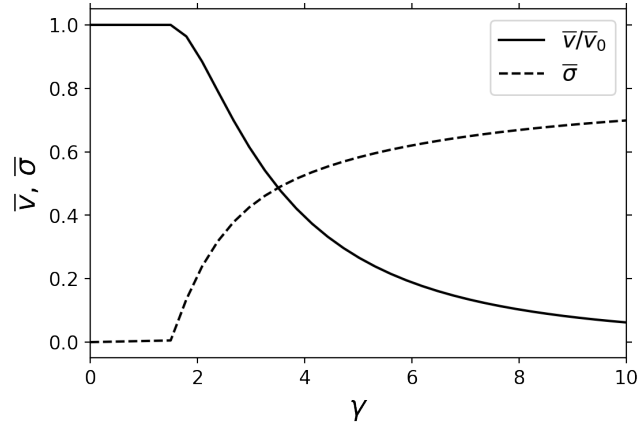


Figure 11: Predictions of the STEPB model for the mean and variance of the final daughter droplet distribution after an initial step-strain deformation. Below a strain of about $\gamma = 1.5$, droplets are not predicted to break. Above that limit, however, increasing initial strain leads to a smaller droplet size \bar{v}/v_0 and higher relative variance $\bar{\sigma}$ in the distribution.

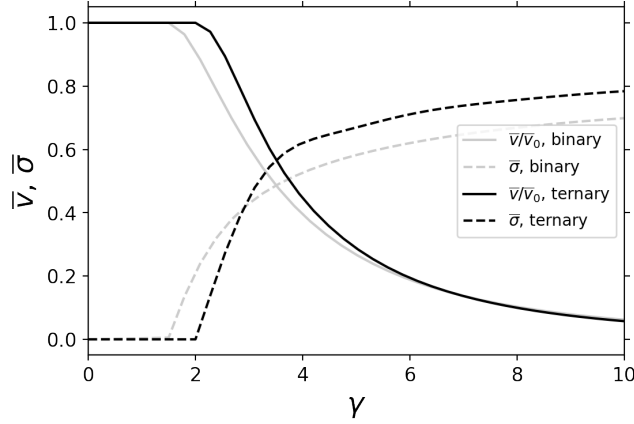


Figure 12: Comparing predictions of the STEPB model with binary/ternary breakup rules. Here, we consider the mean and variance of the final daughter droplet distribution after an initial step-strain deformation. Ternary breakage requires a higher initial strain, but for sufficiently large strain the final droplet size is roughly independent of the binary/ternary breakage rule. At high strains, variance in the final droplet size distribution is greater for the ternary breakup rule.

5 Sample Calculations with Experimental Data

The STEPB model was developed to address a gap in the existing emulsion modeling literature, where droplet breakup in stabilized emulsions is difficult to describe if the deformation is unsteady. In particular, section 4 looked at droplet breakup following step-strain deformation, and it is our view that the STEPB model shows tremendous promise in its ability to leverage simple approximations for capturing complex phenomena relevant to droplet breakup in unsteady deformations.

Outside of unsteady flow conditions, we will make no claims for the conceptual or practical superiority of the STEPB model as presently formulated. In steady simple shear flow, for example, the STEPB model allocates a lot of resources to describing a droplet’s shape and proclivity to breakup - information that can be reasonably inferred from the imposed shear rate alone. At the same time, STEPB allocates very few resources to describing phenomena that are often relevant to the final daughter droplet distribution in steady flow, namely (1) coalescence (where applicable) and (2) complex daughter droplet distributions.

To reinforce this discussion, we will provide a comparison between STEPB predictions and experimental results for oil/water emulsions processed in a cone-mill device [8]. The point of this comparison is to highlight the weaknesses of the STEPB model and to discuss why these weaknesses are less of a liability for the unsteady deformations that STEPB is principally designed to address.

In a recent study by Dubbelboer et al [8], the authors prepared a series of dense emulsions (mayonnaise) from oil, water, vinegar, egg yolk, and salt with varying oil concentration. The components were initially mixed in a Silverson High Shear Mixer, and the droplet size distribution was refined by high shear processing in a cone mill. For an emulsion of 72% oil, $\phi = 0.72$, the authors estimate a surface tension of $\Gamma = 10\text{mN/m}$, an effective viscosity of $\mu^{eff} = 0.18\text{Pa}\cdot\text{s}$, and an initial average droplet diameter of $37\mu\text{m}$. From these, we can estimate a typical droplet relaxation time of $\tau = \mu^{eff}r_0/\Gamma = 3.3 \cdot 10^{-4}\text{s}$. The cone mill effectively exposes droplets to steady shear flow with a shear rate of $\dot{\gamma} = 25000/\text{s}$, which gives us an estimated overall Capillary number of $Ca = 8.5$ and we expect to see significant changes in the droplet size distribution. Our STEPB predictions will assume $\zeta = 0$, and the initial/final droplet size distributions are lifted from figures 3b and 10a of the Dubbelboer report [8].

Numerical solutions of the STEPB model are obtained via the miCDF scheme [25], the principle of which is covered in more detail in appendix A of the present work. In summary, miCDF divides the droplet size distribution into fractions of equal volume and tracks the typical droplet size/shape in each fraction over time. In our view, miCDF is an extremely useful discretization strategy for coupled rheology/PBE problems because (1) large changes in the size distribution do not require re-meshing the size distribution and (2) compared to other “adaptive” methods, miCDF does not lose accuracy when handling a moving reference droplet volume in the shape evolution equation.

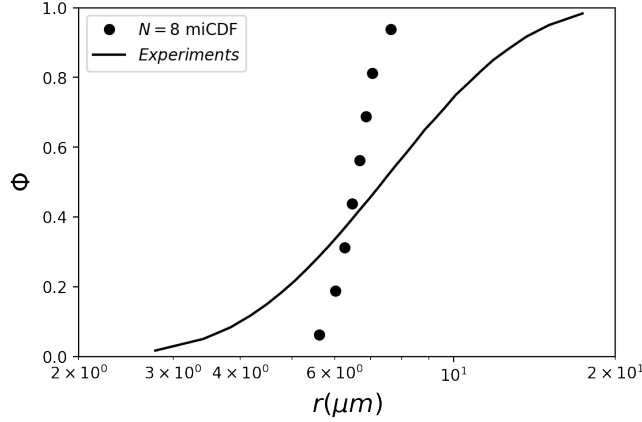


Figure 13: Comparing predictions from the STEPB model against experimental observations for the steady state droplet size distribution (in terms of a cumulative size distribution) for a stabilized oil/water emulsion $\phi = 0.72$ as described in work done by Dubbelboer et. al. [REF]. Note that STEPB captures the typical droplet size reasonably well, but dramatically underestimates the variance in the final distribution.

Having established the context of our simulations, we now compare STEPB predictions for the final droplet size distribution against the results from Dubbelboer et. al. In figure 13, we show that STEPB seems to capture the average droplet size reasonably well, but dramatically underestimates the variance of the distribution.

The broader droplet size distribution observed in experiments shows that the STEPB model is missing important physics relevant to steady simple shear flows, but the general agreement in average droplet size indicates that there are key ideas within STEPB worth building on. In terms of weaknesses, the broader droplet size distribution could be achieved by some combination of (1) directly assigning a broader daughter droplet distribution and/or (2) allowing droplet coalescence to occur. The latter of these two modes is particularly interesting: by allowing coalescence, one can sustain a population of droplets with size above the critical size for breakup. These larger droplets can become highly stretched, facilitating successive generations of droplet breakup and extending the droplet size distribution well below the critical size for breakup at the imposed shear rate. However, for stabilized dense emulsions with an excess of surfactant (such as the mayonnaise used in these experiments) the mechanism for coalescence is unclear, and so complex daughter droplet distributions are a more likely explanation.

To summarize the above, we suggest that figure 13 shows that STEPB accurately identifies a critical capillary number as reflected by the typical droplet size surviving at steady state, but fails to capture the breadth of the droplet size distribution possibly due to the omission of coalescence in the present implementation. However, implementing coalescence in the STEPB model is not obvious: how does one interpret the process of coalescence in terms of ellipsoids alone? If coalescence happens under deformation but not at equilibrium, how should the shape tensor enter into the coalescence rate expression? This is a target for future work, and may require higher-order tensor representations of droplet shape evolution.

Having acknowledged these weaknesses, we remind the reader that the current formulation of the STEPB model was designed to address flows at high Deborah numbers (i.e. closer to step deformation than steady shear). High Deborah number flows could be encountered in contractions/expansion zones for processing equipment and valves, but also in fully resolved turbulent flows for conventional mixers. At high Deborah numbers, droplet breakup is dominated by the strain introduced in a narrow interval of time, and a broad distribution of daughter droplets can be found without direct fine-tuning of the daughter droplet distribution. By contrast, at low Deborah numbers all droplets above a critical size will eventually break, and virtually no droplets below that critical size will break, such that the final daughter droplet distribution bears a direct reflection of what one has assumed about the daughter droplet distribution for individual breakup events.

Since there are already existing models to cover low Deborah number applications [8, 18], poor performance of the STEPB model under steady shear does not seriously detract from its overall

usefulness, in our view. That being said, it should be possible to improve the model so that it performs suitably in both high and low Deborah number flows.

6 Summary and Conclusions

In this paper, we introduced the “shape tensor emulsion population balance” (STEPB) model for coupling the evolution equations on droplet shape and droplet size distribution. The main weaknesses of the model as presently formulated are (1) it is restricted to interpolate the breakup process as a transition from an ellipsoidal parent droplet to a collection of ellipsoidal daughter droplets, (2) it neglects terms related to droplet coalescence, and (3) it relies on a very simple symmetric binary breakup approximation of the daughter droplet size distribution. In spite of these weaknesses, we have shown that the STEPB model yields non-trivial predictions regarding a complex strain-dependent daughter droplet distribution under step-strain deformations. This is a result that would challenge competing emulsion models, and in STEPB it is accomplished with only four parameters; a surface tension Γ , a relaxation time τ , a “slip” parameter ζ , and a kinetic prefactor to breakup α . The slip parameter ζ accounts for non-affine deformation as might occur if the dispersed droplet were of a much higher viscosity than the surrounding medium. Like the viscosity ratio, the slip parameter also controls the critical capillary number in simple shear flow (c.f. appendix B). The kinetic prefactor $\alpha \sim O(1)$ ties the processes of breakup and shape relaxation together, as needed to ensure that the joint relaxation/breakup processes always decrease total surface area.

Looking towards future research with the STEPB modeling framework, there are three main directions that seem worth pursuing in terms of improvements upon the STEPB model itself. In a first direction, there are opportunities to incorporate additional physics into the STEPB model: we can move towards higher-order tensors, readmit droplet coalescence, fine-tune the daughter droplet distribution, add memory into the droplet breakup rate, and so on. In a second direction, by contrast, there are opportunities to pursue further simplifications: we could perhaps use the STEPB model as a benchmark for evaluating the performance of reduced-order models, with complexity in-line with a generalized Doi-Ohta model. Finally, a third research direction (possibly in conjunction with the second) would be to embed the STEPB model (or a simplified variant) into CFD model calculations to better understand and optimize the processes by which dense emulsions are formed in industry applications.

Besides these modeling directions, the STEPB model opens up new opportunities for experimental and computational probing of droplet breakup dynamics in dense emulsions. Most notably, droplet breakup in step deformation appears to be a useful and well-defined problem to consider. It would be interesting to develop experiments or simulations that allow for simultaneous real-time measurement of droplet deformation, stress relaxation, and breakup of dense suspensions at high Capillary numbers.

In all, it is our view that the STEPB model represents a major conceptual advance in the available tools for modeling droplet breakup in dense emulsions and there are many promising directions for follow-up work, through both experimental and computational/theoretical endeavors.

7 Acknowledgments

The authors would like to acknowledge Unilever and the CAFE4DM consortium for funding and technical input. We also acknowledge financial support from the European Research Council under the Horizon 2020 Programme, ERC grant agreement number 740269.

References

References

- [1] Alexandre Afonso, Paulo J Oliveira, FT Pinho, and MA Alves. The log-conformation tensor approach in the finite-volume method framework. *Journal of Non-Newtonian Fluid Mechanics*, 157(1-2):55–65, 2009.

- [2] D Barthes-Biesel and Andreas Acrivos. Deformation and burst of a liquid droplet freely suspended in a linear shear field. *Journal of Fluid Mechanics*, 61(1):1–22, 1973.
- [3] Marco Caggioni, Veronique Trappe, and Patrick T Spicer. Variations of the herschel–bulkley exponent reflecting contributions of the viscous continuous phase to the shear rate-dependent stress of soft glassy materials. *Journal of Rheology*, 64(2):413–422, 2020.
- [4] ME Cates. Reptation of living polymers: dynamics of entangled polymers in the presence of reversible chain-scission reactions. *Macromolecules*, 20(9):2289–2296, 1987.
- [5] CA Coualoglou and Lawrence L Tavlarides. Description of interaction processes in agitated liquid-liquid dispersions. *Chemical Engineering Science*, 32(11):1289–1297, 1977.
- [6] Eric DeGiuli and Matthieu Wyart. Unifying suspension and granular flows near jamming. In *EPJ Web of Conferences*, volume 140, page 01003. EDP Sciences, 2017.
- [7] Masao Doi and Takao Ohta. Dynamics and rheology of complex interfaces. i. *The Journal of chemical physics*, 95(2):1242–1248, 1991.
- [8] Arend Dubbelboer, Jo JM Janssen, Hans Hoogland, Edwin Zondervan, and Jan Meuldijk. Pilot-scale production process for high internal phase emulsions: Experimentation and modeling. *Chemical Engineering Science*, 148:32–43, 2016.
- [9] Salah Aldin Faroughi and Christian Huber. A generalized equation for rheology of emulsions and suspensions of deformable particles subjected to simple shear at low reynolds number. *Rheologica Acta*, 54(2):85–108, 2015.
- [10] Raanan Fattal and Raz Kupferman. Constitutive laws for the matrix-logarithm of the conformation tensor. *Journal of Non-Newtonian Fluid Mechanics*, 123(2-3):281–285, 2004.
- [11] Raanan Fattal and Raz Kupferman. Time-dependent simulation of viscoelastic flows at high weissenberg number using the log-conformation representation. *Journal of Non-Newtonian Fluid Mechanics*, 126(1):23–37, 2005.
- [12] LJ Harrison and FE Cunningham. Factors influencing the quality of mayonnaise: a review. *Journal of food quality*, 8(1):1–20, 1985.
- [13] Martien A Hulsen, Raanan Fattal, and Raz Kupferman. Flow of viscoelastic fluids past a cylinder at high weissenberg number: stabilized simulations using matrix logarithms. *Journal of Non-Newtonian Fluid Mechanics*, 127(1):27–39, 2005.
- [14] Fardin Khabaz, Michel Cloitre, and Roger T Bonnecaze. Particle dynamics predicts shear rheology of soft particle glasses. *Journal of Rheology*, 64(2):459–468, 2020.
- [15] RG Larson. The elastic stress in “film fluids”. *Journal of Rheology*, 41(2):365–372, 1997.
- [16] Ronald G Larson. *Constitutive equations for polymer melts and solutions: Butterworths series in chemical engineering*. Butterworth-Heinemann, 2013.
- [17] PL Maffettone and Mario Minale. Equation of change for ellipsoidal drops in viscous flow. *Journal of Non-Newtonian Fluid Mechanics*, 78(2-3):227–241, 1998.
- [18] Shashank Maindarkar, Arend Dubbelboer, Jan Meuldijk, Hans Hoogland, and Michael Henson. Prediction of emulsion drop size distributions in colloid mills. *Chemical Engineering Science*, 118:114–125, 2014.
- [19] David Julian McClements. Protein-stabilized emulsions. *Current opinion in colloid & interface science*, 9(5):305–313, 2004.
- [20] Robert McGraw. Description of Aerosol Dynamics by the Quadrature Method of Moments. *Aerosol Sci. Technol.*, 27(2):255–265, jan 1997.
- [21] Mario Minale. Models for the deformation of a single ellipsoidal drop: a review. *Rheologica acta*, 49(8):789–806, 2010.

- [22] Paul M Mwasame, Norman J Wagner, and Antony N Beris. On the macroscopic modelling of dilute emulsions under flow. *Journal of Fluid Mechanics*, 831:433–473, 2017.
- [23] Vivek Narsimhan. Shape and rheology of droplets with viscous surface moduli. *Journal of Fluid Mechanics*, 862:385–420, 2019.
- [24] Rajinder Pal. Viscous behavior of concentrated emulsions of two immiscible newtonian fluids with interfacial tension. *Journal of colloid and interface science*, 263(1):296–305, 2003.
- [25] Joseph D Peterson, Ioannis Bagkeris, and Vipin Michael. A new framework for numerical modeling of population balance equations: Solving for the inverse cumulative distribution function. *Chemical Engineering Science*, 259:117781, 2022.
- [26] Joseph D Peterson and ME Cates. A full-chain tube-based constitutive model for living linear polymers. *Journal of Rheology*, 64(6):1465–1496, 2020.
- [27] Spencer Umfreville Pickering. Emulsions. *Journal of the Chemical Society, Transactions*, 91:2001–2021, 1907.
- [28] JM Rallison. The deformation of small viscous drops and bubbles in shear flows. *Annual review of fluid mechanics*, 16(1):45–66, 1984.
- [29] Doraiswami Ramkrishna. *Population balances: Theory and applications to particulate systems in engineering*. Elsevier, 2000.
- [30] Pierre Saramito. A new constitutive equation for elastoviscoplastic fluid flows. *Journal of Non-Newtonian Fluid Mechanics*, 145(1):1–14, 2007.
- [31] Frank Scheffold, Frédéric Cardinaux, and Thomas G Mason. Linear and nonlinear rheology of dense emulsions across the glass and the jamming regimes. *Journal of Physics: Condensed Matter*, 25(50):502101, 2013.
- [32] Jay D Schieber and Andrés Córdoba. Nonequilibrium thermodynamics for soft matter made easy (er). *Physics of Fluids*, 33(8):083103, 2021.
- [33] Natasha Singh and Vivek Narsimhan. Deformation and burst of a liquid droplet with viscous surface moduli in a linear flow field. *Physical Review Fluids*, 5(6):063601, 2020.
- [34] Howard A Stone, BJ Bentley, and LG Leal. An experimental study of transient effects in the breakup of viscous drops. *Journal of Fluid Mechanics*, 173:131–158, 1986.
- [35] Tharwat F Tadros. Emulsions. In *Emulsions*. de Gruyter, 2016.
- [36] Geoffrey Ingram Taylor. The formation of emulsions in definable fields of flow. *Proceedings of the Royal Society of London. Series A, containing papers of a mathematical and physical character*, 146(858):501–523, 1934.
- [37] Alexander Vikhansky and Andrew Splawski. Adaptive multiply size group method for CFD-population balance modelling of polydisperse flows. *Canadian Journal of Chemical Engineering*, 93(8):1327–1334, 2015.
- [38] JA Wieringa, F Vandieren, JJ Janssen, and WG Agterof. Droplet breakup mechanisms during emulsification in colloid mills at high dispersed phase volume fraction. *Chemical engineering research & design*, 74(5):554–562, 1996.
- [39] Dongrong Xu, Jiali Cui, Ravi Bansal, Xuejun Hao, Jun Liu, Weidong Chen, and Bradley S Peterson. The ellipsoidal area ratio: an alternative anisotropy index for diffusion tensor imaging. *Magnetic resonance imaging*, 27(3):311–323, 2009.

A Addition Details on Numerical Methods

In section 4, we will consider calculations for droplets that are initially monodisperse, $n(t = 0, v) = \delta(v - v_0)$, in which case equation 7 yields a solution of the form:

$$n(t, v) = \sum_{i=0}^{\infty} n_i(t) \delta(v - v_0/2^i) \quad (42)$$

where the droplets are delta-distributed at volumes reflecting successive divisions of the starting droplet. Inserting equation 42 into equation 7 and grouping terms at each delta-peak yields the following set of evolution equations:

$$\frac{\partial}{\partial t} n_0 = -g_0 n_0 \quad (43)$$

$$\frac{\partial}{\partial t} n_{i>0} = -g_i n_i + 2g_{i-1} n_{i-1} \quad (44)$$

where $g_i = g(v_i)$. For our purposes, we truncate equation 42 when droplets are small enough that no further breaking takes place within the model.

If the initial droplet size distribution is not delta-distributed, then choosing an appropriate discretization strategy is more difficult. In principle, one could break the initial condition into a finely-resolved set of delta-peaks and repeat the process outlined above, but this will typically be inefficient when the eventual goal is to embed the emulsion model into CFD calculations.

While many discretization strategies may be possible, we will employ our recently devised “method of the Inverse Cumulative Distribution” (miCDF) scheme, which effectively breaks the population into pre-allocated intervals of total volume, and then tracks the median droplet size within each interval. To expand on this summary, we first define a volume density distribution $\phi(v) = vn(v)$ as a simple volume-weighted transformation of the number density distribution. This volume density distribution is conservative, $\int_0^\infty dv \phi(v) = \phi_0$ and as such can be interpreted as a probability density function. From that probability density function, we can define a cumulative distribution function (CDF) $\Phi(v)$:

$$\Phi(v) = \frac{1}{\phi_0} \int_0^v dv' \phi(v') \quad (45)$$

For a given droplet size v , the CDF Φ gives the total volume fraction of droplets with size less than v . Conversely, the inverse CDF, $v(\Phi)$ gives the limiting droplet size needed to contain a specified fraction Φ of the total droplet volume fraction. Note that because $\phi(v) > 0$, $\Phi(v)$ is monotonically increasing in v , as needed for the inverse function to exist. An evolution equation for $v(\Phi)$ is produced by applying the triple product rule:

$$\left(\frac{\partial v}{\partial t} \right)_\Phi = - \left(\frac{\partial v}{\partial \Phi} \right)_t \left(\frac{\partial \Phi}{\partial t} \right)_v = - \frac{1}{\phi} \int_0^v dv' \frac{\partial}{\partial t} \phi(v') \quad (46)$$

Recasting the evolution equation in terms of the inverse CDF can be advantageous whenever there are large changes in the droplet size distribution, but it is not the only method with this property [20, 37]. Where the PBE is coupled to an underlying viscoelastic constitutive equation, however, it is our view that the miCDF discretization strategy is a more natural and more flexible strategy overall.

When the droplet shape is tracked along moving reference droplet size $v^*(t)$, the shape evolution equations 22 and 24 must contain an additional “advection” term to account for changes in shape that occur simply due to changes in the reference droplet size:

$$\left(\frac{\partial \Theta}{\partial t} \right)_{v^*} = \dots + \left(\frac{\partial \Theta}{\partial v} \right)_{v=v^*} \left(\frac{\partial v^*}{\partial t} \right) \quad (47)$$

where the ellipses denote terms previously derived for the fixed droplet volume reference frame (deformation, relaxation, population balances, etc). A moving reference frame of this nature is common to most of the PBE methods considered in coupled CFD/PBE applications, including those based on the popular “Quadrature Method of Moments” QMOM approach [20, 37]. In QMOM, moment evolution equations are closed via an expensive moment inversion approximation that can be accurate for quadrature in v but not especially useful for evaluating derivatives in v , as needed for the moving

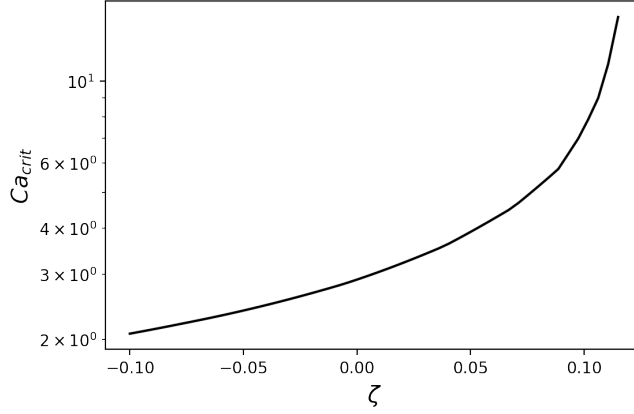


Figure 14: Predictions for the critical capillary number Ca_{crit} of the STEPB model as a function of the slip parameter ζ . With increasing slip, higher shear rates are needed to induce breakup in simple shear; for slip exceeding $\zeta > 0.11$, droplet breakup cannot be achieved at any shear rate.

reference frame in equation 47. By contrast, miCDF avoids the slow moment inversion step and yields a consistent order of accuracy across both number density and shape evolution equations. In our calculations, we rely on simple linear interpolations and trapezoid quadrature schemes for numerical calculations.

B Slip and the Critical Capillary Number

In the STEPB model, we describe droplets as ellipsoids that deform non-affinely in flow with a uniform “slip” factor ζ subtracted against the bulk strain gradient. This slip is partially intended to reflect the influence of varying relative viscosity of the droplet itself and the surrounding medium - where the surrounding medium is less viscous, for example, droplets will resist deformation relative to the background flow [REF]. In dilute emulsions, for example, the “critical capillary number” Ca_{crit} for droplet breakup depends on this viscosity ratio, and even diverges for a viscosity ratio of 4. In keeping with that, we show in figure 14 that Ca_{crit} diverges for $\zeta \sim 0.11$ in the STEPB model. This analogy breaks down for negative values of ζ , where one might hope to represent a low viscosity dispersed phase: in reality, Ca_{crit} is a non-monotonic function of the viscosity ratio, with intermediate viscosity ratios having the lowest Ca_{crit} . This is a potential liability for the STEPB model, but for dense suspensions the effective viscosity in the medium surrounding a droplet is not necessarily the viscosity of the continuous phase.